Inorg. Chem. **2004**, *43*, 1491–1501

Organometallic Oligomers Based on 1,8-Diisocyano-*p*-menthane (dmb): Syntheses and Characterization of the $\{[M(diphos)(dmb)]BF_4\}_n$ and $\{[Pd_2(diphos)_2(dmb)](ClO_4)_2\}_n$ Materials (M = Cu, Ag; diphos = dppe, dppp)

Eric Fournier,[1a] Stéphanie Sicard,[1a] Andreas Decken,[1b] and Pierre D. Harvey*,[1a]

Département de chimie, Université de Sherbrooke, Sherbrooke, PQ, Canada J1K 2R1, and the Department of Chemistry, University of New Brunswick, Fredericton, New Brunswick, Canada E3B 6E2

Received July 7, 2003

A new strategy to synthesize organometallic oligomers is presented and consists of using the title diisocyanide and chelated metal fragments with bis(diphenylphosphine)alkanes. The title materials are synthesized by reacting the $[M(dppe)(BF_4)]$ and $[M_2(dppp)_2](BF_4)_2$ complexes (M = Cu, Ag; dppe = bis(diphenylphosphino)ethane, dppp = bis(diphenylphosphino)propane) with dmb and the Pd_2-bonded d^9–d^9 $Pd_2(dmb)_2Cl_2$ dimer with dppe or dppp. The model compounds $[M(diphos)(CN\text{-}t\text{-}Bu)_2]BF_4$ (M = Cu, Ag) and $[Pd_2(diphos)_2(CN\text{-}t\text{-}Bu)_2](ClO_4)_2$ (diphos = dppe, dppp) have been prepared and characterized as well for comparison purposes. Three of the model compounds were also characterized by X-ray crystallography to establish the diphosphine chelating behavior. The materials are amorphous and have been characterized from the measurements of the intrinsic viscosity, DSC, TGA, and XRD, as well as their capacity for making stand-alone films. The intrinsic viscosity data indicate that the Cu and Pd_2 materials are oligomeric in solution (~8–9 units), while the Ag materials are smaller. For $\{[Cu(dppe)(dmb)]BF_4\}_n$, a glass transition is reproducibly observed at about 82 °C (ΔC_p = 0.43 J/(g deg)), which suggests that these materials are polymeric in the solid state. The Cu and Ag species are luminescent in the solid state at room temperature exhibiting λ_{max} and τ_e (emission lifetime) around 480–550 nm and 18–48 μs, respectively, while the Pd_2 species are not luminescent under these conditions. During the course of this study, the unsaturated $[M_2(dppp)_2](BF_4)_2$ starting materials (M = Cu, Ag) were prepared, one of which (M = Ag) was characterized by crystallography. The bridging behavior of the dppp ligand in this case contrasts with the chelating behavior seen for the saturated $[Cu(dppp)(CN\text{-}t\text{-}Bu)_2]BF_4$ complex.

Introduction

The title bridging ligand (Chart 1) has become a highly versatile assembling building block over the past 30 years.[2] Indeed, this ligand is well-known for the synthesis of binuclear complexes, although some examples of tri- and tetranuclear dmb-containing species have also been reported.[3]

Recently, this ligand was used for the first time in the synthesis of the organometallic polymers $\{M(dmb)_2^+\}_n$ (M = Cu, Ag; Chart 2),[4] which have been fully characterized by X-ray diffraction techniques and molecular weight measurements (M_n and M_w). Applications in the areas of semi- and photoconductivity and photovoltaic cells were reported as well.[4d]

Chart 1

dmb (*U*-conformation) dmb (*Z*-conformation)

The uniqueness of these new materials is that they keep their polymeric, or at least oligomeric, nature in solution[4b,e] and can use both the *U*- and *Z*-conformations for dmb to form various isomeric 1-D polymers.[4c] On the other hand, the related and more flexible diisocyanide ligand tmb (2,5-

* To whom correspondence should be addressed. E-mail: p.harvey@Usherbrooke.ca. Tel: (819) 821-7092 or (819) 821-8000 ext 8000, ext 2005. Fax: (819) 821-8017.

(1) (a) Université de Sherbrooke. (b) University of New Brunswick.

(2) Harvey, P. D. *Coord. Chem. Rev.* **2001**, *219*, 17, and references therein.

10.1021/ic034780z CCC: $27.50
Published on Web 01/13/2004

Chart 2

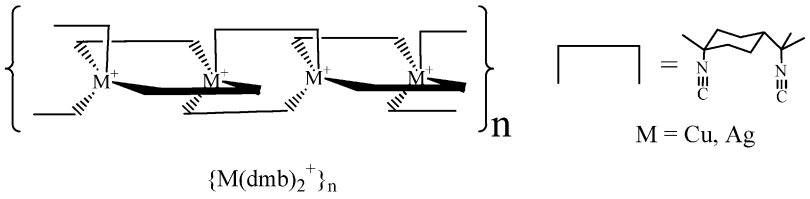

$\{M(dmb)_2^+\}_n$

Chart 3

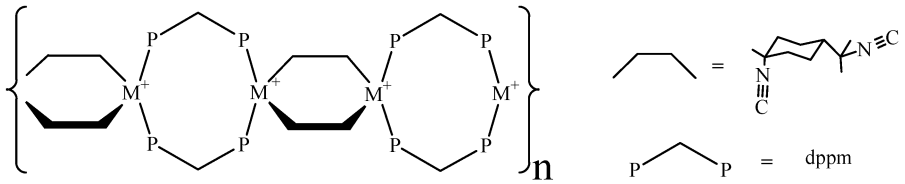

$\{M_2(dppm)_2(dmb)_2^{2+}\}_n$; M = Cu, Ag

Chart 4

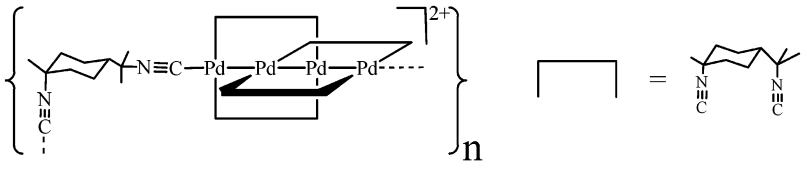

$\{Pd_4(dmb)_4(dmb)^{2+}\}_n$

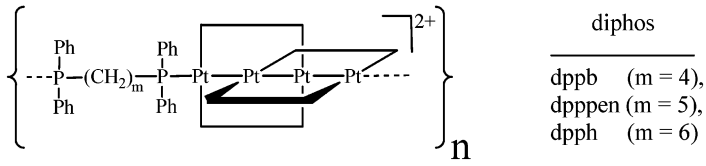

$\{Pt_4(dmb)_4(diphos)^{2+}\}_n$

dimethyl-2′,5′-diisocyanohexane) produces 2- or 3-D polymer structures, as reported for polymers of the type $\{Ag(tmb)^+\}_n$ and $\{Ag_2(tmb)_3^{2+}\}_n$.[5] The two strategies for the synthesis of 1-D materials that retain their oligomeric or polymeric nature in solution are the use of two dmb bridges between the metallic fragments (such as fragment = M^{+} [4] and $M_2(dppm)_2^{2+}$ [6] with M = Cu, Ag; dppm = bis(diphenylphosphino)methane; Chart 3) and of axially functionalizable metallic fragments exhibiting strong (and not so labile) $M-L_{axial}$ bonding (such as Pd−CNR and Pd−P; Chart 4).[3a,b] In the examples illustrated below, M_4 species are bridged together by dmb (*Z*-conformer), or by flexible diphosphine ligands, leading to crystalline and amorphous materials, respectively.[7]

We now wish to report the synthesis and characterization of a series of new oligomers built upon chelated diphosphine metallic fragments, such as "$M(diphos)^{+}$" and "$Pd_2(diphos)_2^{2+}$" (M = Cu, Ag; diphos = dppe, dppp), and the bridging dmb ligands. This approach is novel and is based on the intramolecular steric hindrance and ring stress that prevent the dimer formation. The materials are characterized from the measurements of the intrinsic viscosity, DSC, TGA, XRD, luminescence spectroscopy, and the capacity of forming stand-alone film and compared to model compounds such as the mononuclear complexes $[M(dppe)(CN\text{-}t\text{-}Bu)_2]BF_4$ (M = Cu, Ag) and $[M(dppp)(CN\text{-}t\text{-}Bu)_2]BF_4$ and Pd_2-bonded dimers $[Pd_2(diphos)_2(CN\text{-}t\text{-}Bu)_2](ClO_4)_2$ (diphos = dppe, dppp). In the area of coordination polymers and

(3) (a) Zhang, T.; Drouin, M.; Harvey, P. D. *Inorg. Chem.* **1999**, *38*, 1305. (b) Zhang, T.; Drouin, M.; Harvey, P. D. *Inorg. Chem.* **1999**, *38*, 957. (c) Fortin, D.; Drouin, M.; Harvey, P. D.; Herring, F. G.; Summers, D. A.; Thompson, R. C. *Inorg. Chem.* **1999**, *38*, 1253. (d) Zhang, T.; Drouin, M.; Harvey, P. D. *Inorg. Chem.* **1999**, *38*, 4928. (e) Sykes, A. G.; Mann, K. R. *Inorg. Chem.* **1990**, *29*, 4449. (f) Sykes, A. G.; Mann, K. R. *J. Am. Chem. Soc.* **1988**, *110*, 8252. (g) Sykes, A. G.; Mann, K. R. *J. Am. Chem. Soc.* **1990**, *112*, 7247. (h) Harvey, P. D.; Drouin, M.; Michel, A.; Perreault, D. *J. Chem. Soc., Dalton Trans.* **1993**, 1365.

(4) (a) Perreault, D.; Drouin, M.; Michel, A.; Harvey, P. D. *Inorg. Chem.* **1992**, *31*, 3688. (b) Fortin, D.; Drouin, M.; Turcotte, M.; Harvey, P. D. *J. Am. Chem. Soc.* **1997**, *119*, 531. (c) Fortin, D.; Drouin, M.; Harvey, P. D. *J. Am. Chem. Soc.* **1998**, *120*, 5351. (d) Fortin, D.; Drouin, M.; Harvey, P. D. *Inorg. Chem.* **2000**, *39*, 2758. (e) Turcotte, M.; Harvey, P. D. *Inorg. Chem.* **2002**, *41*, 2971.

(5) (a) Guitard, A.; Mari, A.; Beauchamp, A. L.; Dartiguenave, Y.; Dartiguenave, M. *Inorg. Chem.* **1983**, *22*, 1603. (b) Dartiguenave, M.; Dartiguenave, A.; Mari, A.; Guitard, A.; Olivier, M.-J.; Beauchamp, A. L. *Can. J. Chem.* **1988**, *66*, 2386.

(6) (a) Fournier, E.; Lebrun, F.; Decken, A.; Harvey, P. D. Submitted for publication. (b) Lebrun, F. M.Sc. Dissertation, Université de Sherbrooke, 2001.

(7) Examples of of diphosphine-linked cluster units have been reported. See for instance: (a) Ferguson, G.; Hourintane, R.; Spalding, T. R. *Acta Crystallogr., Sect. C* **1991**, *47*, 544. (b) Tanase, T.; Horiuchi, T.; Yamamoto, Y.; Kobayashi, K. *J. Organomet. Chem.* **1992**, *440*, 1. (c) Hattersley, A. D.; Housecroft, C. E.; Rheingold, A. L. *Inorg. Chim. Acta* **1999**, *289*, 149. (d) Ferrer, M.; Rosell, O.; Seco, M.; Soler, M.; Font-Bardia, M.; Solans, X.; de Montauzon, D. *J. Organomet. Chem.* **2000**, *598*, 215.

Table 1. Numbering of the Investigated Compounds

compd	no.
$[M(dppe)(CN\text{-}t\text{-}Bu)_2]BF_4$	M = Cu, **1**; M = Ag, **2**
$[Cu(dppp)(CN\text{-}t\text{-}Bu)_2]BF_4$	3
$[Pd_2(dppe)_2(CN\text{-}t\text{-}Bu)_2](ClO_4)_2$	4
$[Pd_2(dppp)_2(CN\text{-}t\text{-}Bu)_2](ClO_4)_2$	5
$\{[M(dppe)(dmb)]BF_4\}_n$	M = Cu, **6**; M = Ag, **7**
$\{[M(dppp)(dmb)]BF_4\}_n$	M = Cu, **8**; M = Ag, **9**
$\{[Pd_2(dppe)_2(dmb)](ClO_4)_2\}_n$	10
$\{[Pd_2(dppp)_2(dmb)](ClO_4)_2\}_n$	11

oligomers of Cu(I) and Ag(I) exhibiting luminescence, only a few examples have been reported so far.[8] A compound numbering is provided in Table 1.

Experimental Section

Materials. dmb, $Pd_2(CN\text{-}t\text{-}Bu)_4Cl_2$, $Pd_2(dmb)_2Cl_2$, and $[Cu(NCMe)_4]BF_4$ were synthesized according to literature procedures.[9] The $[M(dppe)(BF_4)]$ starting materials (M = Cu, Ag) were prepared in the same way as $[Ag(dppe)(ClO_4)]$,[10] except that $AgClO_4$ was replaced by either $AgBF_4$ or $[Cu(CNMe)_4]BF_4$. The $[M_2(dppp)_2](BF_4)_2$ dimers were synthesized in the same manner as the complexes $[Cu_2(dppp)_2](ClO_4)_2$[11] and $[Ag_2(dppb)_2](NO_3)_2$[12] (dppb = bis(diphenylphosphino)butane), except that dppp was used instead of dppb, $[Cu(NCMe)_4]BF_4$ instead of $[Cu(NCMe)_4]ClO_4$, and $AgBF_4$ instead of $AgNO_3$. The identity of the $[M_2(dppp)_2](BF_4)_2$ starting materials was confirmed by X-ray structure determination methods for M = Ag (see below and the Supporting Information). $Cu(BF_4)_2 \cdot H_2O$, $AgBF_4$, *t*-BuNC, dppe, and dppp were purchased from Aldrich and were used as received. The solvents acetone (Fisher), acetonitrile (Anachemia), dichloromethane (ACP), diethyl ether (ACP), and butyronitrile (Aldrich) were purified according to published procedures.[13] The Cu and Ag compounds and Pd_2 species were prepared as BF_4^- and ClO_4^- salts, respectively. The Pd_2 species were originally prepared as BF_4^- salts, but the use of ClO_4^- ion gave better chemical analysis. *The handling of perchlorate salts of organometallic cations represents a potential explosive hazard. The use of small amounts is recommended.*

$[Cu(dppe)(CN\text{-}t\text{-}Bu)_2]BF_4$ (1). $[Cu(dppe)(BF_4)]$ (601.3 mg, 1.09 mmol) was dissolved in 150 mL of degassed acetone. A 496 μL (4.38 mmol) volume of *t*-BuNC was added dropwise using a microsyringe. The solution was stirred for 1 h and then evaporated. The white powder was dissolved in a minimum amount of dichloromethane prior to adding 100 mL of diethyl ether to precipitate a white solid, which was filtered out and dried in vacuo. Yield: 60% (470 mg). ^{1}H NMR (CD_2Cl_2): δ 7.57−7.42 (m, 20H, Ph), 2.43 (m, 4H, CH_2), 1.38 (s, 18H, CH_3). $^{31}P\{^1H\}$ NMR (CD_2Cl_2): δ −7.58. $^{13}C\{^1H\}$ NMR (CD_2Cl_2): δ 132.7, 132.6, 131.0, 57.7, 30.1, 26.0. IR (KBr): ν 1059 (BF_4), 2170 cm^{-1} (C≡N). Raman (neat solid): ν 2172 cm^{-1} (C≡N). UV−vis (CH_3CN): 222 (44 500), 272 nm (27 500 M^{-1} cm^{-1}).

$[Ag(dppe)(CN\text{-}t\text{-}Bu)_2]BF_4$ (2). $[Ag(dppe)(BF_4)]$ (1.16 g, 1.96 mmol) was dissolved in 100 mL of degassed acetone. A 442 μL (3.91 mmol) volume of *t*-BuNC was added dropwise using a microsyringe. The solution was stirred for 2 h and then reduced to 20 mL volume in vacuo. A 150 mL volume of diethyl ether was added to precipitate the product, which was filtered out and dried. Yield: 88% (1.49 g). ^{1}H NMR (CD_2Cl_2): δ 7.49−7.36 (m, 20H, Ph), 2.43 (m, 4H, CH_2P), 1.48 (s, 18H, CH_3). $^{31}P\{^1H\}$ NMR (CD_2Cl_2): δ 3.38. $^{13}C\{^1H\}$ NMR (CD_2Cl_2): δ 141.2, 132.7, 130.8, 129.3, 57.4, 30.0, 24.9. IR (KBr): ν 2183 (C≡N), 1057 cm^{-1} (BF_4). Raman (neat solid): ν 2184 cm^{-1} (C≡N). UV−vis (CH_3CN): 222 (44 500), 270 nm (30 300 M^{-1} cm^{-1}).

$[Cu(dppp)(CN\text{-}t\text{-}Bu)_2]BF_4$ (3). $[Cu_2(dppp)_2](BF_4)_2$ (301 mg, 0.263 mmol) was dissolved in 100 mL of degassed acetone. A 150 μL (1.33 mmol) volume of *t*-BuNC was added dropwise using a microsyringe. The solution was stirred for 1 h and then evaporated. The white powder was dissolved in a minimum amount of dichloromethane prior to addition of 100 mL of diethyl ether to precipitate a white solid. The solid was filtered out and dried in vacuo. Yield: 77% (301.6 mg). ^{1}H NMR (CD_2Cl_2): δ 7.49−7.36 (m, 20H, Ph), 2.40 (m, 4H, CH_2P), 1.93 (m, 2H, CCH_2C) 1.35 (s, 18H, CH_3). $^{31}P\{^1H\}$ NMR (CD_2Cl_2): δ −8.21. $^{13}C\{^1H\}$ NMR (CD_2Cl_2): δ 132.6, 130.8, 129.1, 30.1, 27.8, 19.1, 18.0. IR (KBr): ν 1061 (BF_4), 2172 cm^{-1} (C≡N). Raman (neat solid): ν 2171 cm^{-1} (C≡N). UV−vis (CH_3CN): 222 (43 900), 274 nm (27 200 M^{-1} cm^{-1}).

$\{[Cu(dppe)(dmb)]BF_4\}_n$ (6). $[Cu(dppe)(BF_4)]$ (609 mg, 1.11 mmol) was dissolved in 70 mL of degassed acetone. A 425 mg (2.22 mmol) amount of dmb was dissolved in 200 mL of degassed acetone in another flask. Both solutions were cooled to 0 °C, and the dmb solution was added dropwise to the dimer solution. The mixture was stirred for 2 h and then reduced to 15 mL volume in vacuo. A 150 mL volume of diethyl ether was added to precipitate the product, which was filtered out and dried. Yield: 57.5% (472 mg). ^{1}H NMR (CD_2Cl_2): δ 7.50−7.40 (m, 20H, Ph), 2.42 (m, 4H, CH_2P), 1.83−1.11 (m, 18H, for 1.04 dmb). $^{31}P\{^1H\}$ NMR (CD_2Cl_2): δ 7.68. $^{13}C\{^1H\}$ NMR (CD_2Cl_2): δ 141.5, 132.6, 131.0, 129.5, 62.8, 60.5, 44.9, 37.3, 29.3, 26.5, 25.6, 22.8. IR (KBr): ν 2174 (C≡N), 1070 cm^{-1} (BF_4). Raman (neat solid): ν 2173 cm^{-1} (C≡N). Anal. Calcd for $C_{38}H_{42}N_2P_2BF_4Cu$ + 0.04 dmb: C, 62.53; H, 5.82; N, 3.94. Found: C, 62.70; H, 6.19; N, 3.92. UV−vis (CH_3CN): 222 (43 600), 270 nm (27 900 M^{-1} cm^{-1}).

$\{[Ag(dppe)(dmb)]BF_4\}_n$ (7). $[Ag(dppe)(BF_4)]$ (272 mg, 0.230 mmol) was dissolved in 70 mL of degassed acetone. A 86.8 mg (4.56 mmol) amount of dmb was dissolved in 200 mL of degassed acetone in another flask. Both solutions were cooled to 0 °C, and the dmb solution was added dropwise to the dimer solution. The mixture was stirred for 2 h and then reduced to 15 mL volume in vacuo. A 150 mL volume of diethyl ether was added to precipitate the product, which was filtered out and dried. Yield: 90% (323 mg). ^{1}H NMR (CD_2Cl_2): δ 7.47−7.32 (m, 20H, Ph), 2.41 (m, 4H, CH_2P), 2.00−1.81 (m, 6H, dmb) 1.54−1.28 (m, 12H, for 1.21 dmb).

(8) (a) Zhang, J.; Xiong, R. G.; Chen, X. T.; Che, C.-M.; Xue, Z.; You, X.-Z. *Organometallics* **2001**, *20*, 4118. (b) Liu, Q.-X.; Xu, F.-B.; Li, Q.-S.; Zang, X.-B.; Leng, Y. L.; Chou, Z.-Z. Zhang, *Organometallics* **2003**, *22*, 309. (c) Zhang, J.; Xiong, R.-G.; Chen, X.-T.; Xue, Z.; Peng, S.-M.; You, X.-Z. *Organometallics* **2002**, *21*, 235. (d) Sun, D.; Cao, R.; Weng, J.; Hong, M.; Liang, Y. *J. Chem. Soc., Dalton Trans.* **2002**, 291. (e) Tong, M.-L.; Shi, X.-M. Chen, *New. J. Chem.* **2002**, *26*, 814. (f) Zheng, S.-L.; Tong, M.-L.; Tan, S.-D.; Wang, Y.; Shi, J.-X.; Tong, Y.-X.; Lee, H. K.; Chen, X.-M. *Organometallics* **2001**, *20*, 5319. (g) Henary, M.; Wootton, J. L.; Khan, S. I.; Zink, J. I. *Inorg. Chem.* **1997**, *36*, 796.

(9) (a) For $Pd_2(CN\text{-}t\text{-}Bu)_2Cl_2$, see: Yamamoto, Y.; Yamazaki, H. *Bull. Chem. Soc. Jpn.* **1985**, *58*, 1843. Otsuka, S.; Tatsuno, Y.; Ataka, K. *J. Am. Chem. Soc.* **1971**, *93*, 6705. (b) For dmb see: Weber, W. D.; Gokel, G. W.; Ugi, I. K. *Angew. Chem., Int. Ed. Engl.* **1972**, *11*, 530. (c) For $Pd_2(dmb)_2Cl_2$ see: Perreault, D.; Drouin, M.; Michel, A.; Harvey, P. D. *Inorg. Chem.* **1992**, *31*, 2740. (d) For $[Cu(NCMe)_4]BF_4$ see: Diez, J.; Gamasa, M. P.; Gimeno, J.; Tiripicchio, A.; Tiripicchio Camellini, M. *J. Chem. Soc., Dalton Trans.* **1987**, 1275.

(10) Coronas, J. M.; Rossel, O.; Sales, J. *J. Organomet. Chem.* **1976**, *121*, 265.

(11) Kitagawa, S.; Kondo, M.; Katawa, S.; Wada, S.; Mackawa, M.; Munakata, M. *Inorg. Chem.* **1995**, *34*, 1455.

(12) Ruina, Y.; Yimin, H.; Baoyu, X.; Dongmei, W.; Douman, *J. Transition Met. Chem.* **1996**, *21*, 28.

(13) (a) Perrin, D. D.; Armarego, W. L. F.; Perrin, D. R. *Purification of laboratory Chemicals* Pergamon: Oxford, U.K., 1966. (b) Gordon, A. J.; Ford, R. A. *The Chemist's Companion, a Handbook of Practical Data, Techniques, and References* Wiley: New York, 1972; p 436.

$^{31}P\{^1H\}$ NMR (CD_2Cl_2): δ 4.49. $^{13}C\{^1H\}$ (CD_2Cl_2): δ 143.8, 143.3, 132.7, 131.0, 129.5, 63.2, 60.7, 44.1, 36.91, 29.0, 27.0, 25.1, 22.7. IR (KBr): ν 2180, 2133 (C≡N), 1058 cm^{-1} (BF_4). Raman (neat solid): ν 2178 cm^{-1} (C≡N). Anal. Calcd for $C_{38}H_{42}N_2P_2BF_4Ag$ + 0.21 dmb: C, 59.11; H, 5.60; N, 4.12. Found: C, 59.14; H, 5.61; N, 4.08. UV−vis (CH_3CN): 222 (38 600), 270 nm (32 200 M^{-1} cm^{-1}).

{[Cu(dppp)(dmb)]BF_4}$_n$ (8). ([Cu_2(dppp)$_2$](BF_4)$_2$) (312 mg, 0.227 mmol) was dissolved in 70 mL of degassed acetone. A 109.3 mg (5.68 mmol) amount of dmb was dissolved in 150 mL of degassed acetone in another flask. Both solutions were cooled to 0 °C, and the dmb solution was added dropwise to the dimer solution. The mixture was stirred for 1 h and then reduced to 20 mL volume in vacuo. Then 150 mL of diethyl ether was added to precipitate the product, which was filtered out and dried. Yield: 92% (385 mg). ^1H NMR (CD_2Cl_2): δ 7.40−7.40 (m, 20H, Ph), 2.41 (m, 4H, CH_2P), 1.86−1.81 (m, 4H, dmb + CCH_2C dppp) 1.63−1.05 (m, 16H, for 1.13 dmb). $^{31}P\{^1H\}$ NMR (CD_2Cl_2): δ −8.17. $^{13}C\{^1H\}$ NMR (CD_2Cl_2): δ 133.8, 132.5, 130.7, 129.2, 63.4, 61.0, 45.5, 37.2, 29.2, 27.8, 22.8, 18.9. IR (KBr): ν 2168 (C≡N), 1057 cm^{-1} (BF_4). Raman (neat solid): ν 2171 cm^{-1} (C≡N). Anal. Calcd for $C_{39}H_{44}N_2P_2BF_4Cu$ + 0.13 dmb: C, 62.20; H, 6.29; N, 3.72. Found: C, 62.65; H, 6.29; N, 3.67. UV−vis (CH_3CN): 222 (38 900), 270 nm (23 400 M^{-1} cm^{-1}).

{[Ag(dppp)(dmb)]BF_4}$_n$ (9). The dimer [Ag_2(dppp)$_2$](BF_4)$_2$ (572 mg, 0.492 mmol) was dissolved in 100 mL of degassed acetone. A 280 mg (1.48 mmol) amount of dmb was dissolved in 200 mL of degassed acetone in another flask. Both solutions were cooled to 0 °C, and the dmb solution was added dropwise to the dimer solution. The mixture was stirred for 2 h and then reduced to 30 mL volume in vacuo. A 150 mL volume of diethyl ether was added to precipitate the product, which was filtered out and dried. Yield: 96% (758 mg). ^1H NMR (CD_2Cl_2): δ 7.39−7.23 (m, 20H, Ph), 2.41 (m, 4H, CH_2P), 2.03−1.91 (m, 4H, for 1.1 dmb) 1.68−1.48 (m, 18H, dmb + CCH_2C dppp). $^{31}P\{^1H\}$ NMR (CD_2Cl_2): δ −1.30. $^{13}C\{^1H\}$ NMR (CD_2Cl_2): δ 144.2, 143.5, 133.5, 132.6, 130.7, 129.3, 63.3, 60.6, 43.9, 36.9, 28.8, 27.1, 22.6, 18.9. IR (KBr): ν 2185, 2130 (C≡N), 1055 cm^{-1} (BF_4). Raman (neat solid): ν 2188 cm^{-1} (C≡N). Anal. Calcd for $C_{39}H_{44}N_2P_2BF_4Ag$ + 0.1 dmb: C, 59.14; H, 5.65; N, 3.77. Found: C, 59.14; H, 5.61; N, 4.08. UV−vis (CH_3CN): 222 (40 300), 272 nm (33 700 M^{-1} cm^{-1}).

{[Pd_2(dppe)$_2$(CN-*t*-Bu)$_2$](ClO_4)$_2$}$_n$ (4). [Pd_2(CN-*t*-Bu)$_4$$Cl_2$] (37 mg, 0.06 mmol) was dissolved in 50 mL of acetonitrile in the dark under N_2 atmosphere, and 13 mg (0.13 mmol) of $LiClO_4$ was added to the mixture. A 48 mg (0.12 mmol) amount of dppe was dissolved in 50 mL of acetonitrile in another flask. The dppe solution was added dropwise to the dimer solution. The mixture was stirred for 2 h and then reduced to 10 mL volume in vacuo. A 100 mL volume of diethyl ether was added to precipitate the product, which was filtered out and dried. N.B.: This compound must be prepared fresh prior to each analysis; it is unstable, even under inert atmosphere in the dark. Yield: 78% (64.2 mg). ^1H NMR (CD_3CN): δ 7.59−7.16 (m, 40H, Ph), 2.53 (m, 8H, CH_2P), 1.68 (s, 18H, CH_3). $^{13}C\{^1H\}$ NMR (CD_2Cl_2): δ 148.2, 131.7, 130.7, 129.2, 56.4, 30.0, 23.9. $^{31}P\{^1H\}$: 44.6 (d, J = ∼0) 57.0 (d, J = ∼0). IR (KBr): ν 2179 cm^{-1} (C≡N). Mass spec FAB (m/z): 1010 (Pd_2(dppe)$_2$; 1009.7), 1093 (Pd_2(dppe)$_2$(CN-*t*-Bu); 1092.8). UV−vis (CH_3CN): 420 nm (28 600 M^{-1} cm^{-1}).

{[Pd_2(dppp)$_2$(CN-*t*-Bu)$_2$](ClO_4)$_2$}$_n$ (5). Under inert atmosphere in the dark, {[Pd_2(CN-*t*-Bu)$_4$$Cl_2$] (15 mg, 0.024 mmol) was dissolved in 50 mL of acetonitrile and 5.4 mg (0.051 mmol) of $LiClO_4$. A 21.1 mg (0.051 mmol) amount of dppp was dissolved in 50 mL of acetonitrile in another flask. The dppp solution was added dropwise to the dimer solution. The mixture was stirred for 2 h and then reduced to 10 mL volume in vacuo. A 100 mL volume of diethyl ether was added to precipitate the product, which was filtered out and dried. N.B.: This compound must be prepared fresh prior to each analysis; it is unstable, even under inert atmosphere in the dark. Yield: 92% (32.3 mg). ^1H NMR (CD_3CN): δ 7.85−7.01 (m, 40H, Ph), 2.55 (m, 8H, CH_2P), 1.77 (m, 4H, CH_2CH_2P), 1.61 (s, 18H, CH_3). $^{31}P\{^1H\}$ NMR (CD_3CN): δ −5.62 (d, J = ∼28), 10.25 (d, J = ∼28). $^{13}C\{^1H\}$ NMR (CD_3CN): δ 141.8, 131.5, 129.5, 128.9, 57.5, 28.9, 27.6, 18.3. IR (KBr): ν 2179 cm^{-1} (C≡N). Mass spec FAB (m/z): 1038 (Pd_2(dppp)$_2$; 1037.7), 1120 (Pd_2(dppp)$_2$(CN-*t*-Bu); 1120.9), 1303 ((Pd_2(dppp)$_2$(CN-*t*-Bu)(ClO_4); 1303.4). UV−vis (CH_3CN): 414 nm (26 000 M^{-1} cm^{-1}).

{[Pd_2(dppe)$_2$(dmb)](ClO_4)$_2$}$_n$ (10). Under inert atmosphere in the dark, [Pd_2(dmb)$_2$$Cl_2$] (19 mg, 0.029 mmol) and 9.8 mg (0.092 mmol) of $LiClO_4$ were dissolved in 50 mL of acetonitrile. The solution was stirred for 1 h. A 22.8 mg (0.057 mmol) amount of dppe was dissolved in 50 mL of acetonitrile in another flask. The dppe solution was added dropwise to the dimer solution. The mixture was stirred for 2 h and then reduced to 10 mL volume in vacuo. A 100 mL volume of diethyl ether were added to precipitate the product, which was filtered out and dried. Yield: 79% (32.0 mg). ^1H NMR (CD_3CN): δ 7.56−6.98 (m, 40H, Ph), 2.65 (m, 8H, CH_2P), 2.05−1.15 (m, 18H, dmb). $^{31}P\{^1H\}$ NMR (CD_3CN): δ −5 (d), 10 (d). $^{13}C\{^1H\}$ NMR (CD_3CN): δ 148.5, 142.2, 131.5, 131.8, 128.5, 65.2, 63.7, 44.2, 35.3, 27.8, 26.5, 24.9, 21.6. IR (KBr): ν 2170 cm^{-1} (C≡N). Mass spec FAB (m/z): 1010 (Pd_2(dppe)$_2$; 1009.7), 1199 (Pd_2(dppp)$_2$(dmb); 1199.9). Anal. Calcd for $C_{64}H_{66}N_2Pd_2P_4Cl_2O_8$: C, 54.95; H 4.76; N 2.00. Found: C, 52.67; H 4.76; N 2.06. UV−vis (CH_3CN): 412 nm (28 000 M^{-1} cm^{-1}).

{[Pd_2(dppp)$_2$(dmb)](ClO_4)$_2$}$_n$ (11). Under inert atmosphere in the dark, [Pd_2(dmb)$_2$$Cl_2$] (29 mg, 0.044 mmol) and 6.3 mg (0.059 mmol) of $LiClO_4$ were dissolved in 50 mL of acetonitrile. The solution was stirred 1 h. A 36.0 mg (0.087 mmol) amount of dppp was dissolved in 50 mL of acetonitrile in another flask. The dppp solution was added dropwise to the dimer solution. The mixture was stirred for 2 h and then reduced to 10 mL volume in vacuo. A 100 mL volume of diethyl ether was added to precipitate the product, which was filtered out and dried in the dark. Yield: 86% (53.6 mg). ^1H NMR (CD_3CN): δ 7.53−7.03 (m, 40H, Ph), 2.58 (m, 8H, CH_2P), 2.10 (m, 4H, CH_2CH_2P), 201−0.98 (m, 18H, dmb). $^{31}P\{^1H\}$: −5.72 (d, J = ∼25 Hz), 10.38 (d, J = ∼25 Hz). $^{13}C\{^1H\}$ NMR (CD_3CN): δ 148.5, 142.2, 131.5, 131.8, 128.5, 65.2, 63.7, 61.9, 44.9, 37.6, 28.2, 27.7, 23.8, 17.9. IR (KBr): ν 2170 cm^{-1} (C≡N). Mass spec FAB (m/z): 1038 (Pd_2(dppp)$_2$; 1037.9), 1227.3 (Pd_2(dppp)$_2$(dmb); 1227.2). Anal. Calcd for $C_{66}H_{70}N_2Pd_2Cl_2O_8$: C, 55.56; H 4.94; N 1.96. Found: C, 52.12; H 5.14; N 2.08. UV−vis (CH_3CN): 414 nm (25 700 M^{-1} cm^{-1}).

Apparatus. All NMR spectra were acquired with a Bruker AC-300 spectrometer (^1H 300.15 MHz, ^{13}C 75.48 MHz, ^{31}P 121.50 MHz) using the solvent as chemical shift standard, except in ^{31}P NMR, where the chemical shifts are relative to D_3PO_4 85% in D_2O. All chemical shifts (δ) and coupling constants (J) are given in ppm and hertz, respectively. The IR spectra were acquired on a Bomem FT-IR MB series spectrometer equipped with a baseline-diffused reflectance. The emission spectra were measured on a Spex Fluorolog II spectrofluorometer using a HgXe excitation lamp. The emission lifetimes were measured with a nanosecond N_2 laser system from PTI model GL-3300 pumping a dye laser model GL-302. The glass transition temperatures (T_g) were measured using a Perkin-Elmer 5A DSC7 instrument equipped with a thermal controller 5B TAC 7/DS. Calibration standards were water and indium. The FT-Raman spectra were acquired on a Bruker RFS

100/S spectrometer. XRD (X-ray powder diffraction) data were acquired on a Rigaku/USA Inc. diffractometer with a copper anode operating under a 30 mA current and a 40 kV tension. TGA were acquired on a TGA 7 of Perkin-Elmer instrument between 50 and 650 °C at 3°/min under nitrogen atmosphere.

Crystallography. All thee crystals were grown by vapor diffusion using acetone−*tert*-butyl methyl ether at 23 °C. Single crystals were coated with Paratone-N oil, mounted using a glass fiber, and frozen in the cold nitrogen stream of the goniometer. A hemisphere of data was collected on a Bruker AXS P4/SMART 1000 diffractometer located at the University of New Brunswick using ω and θ scans with a scan width of 0.3° and using exposure times of 30 s for $[Cu(dppe)(CN\text{-}t\text{-}Bu)_2]BF_4$ (**1**), 10 s for $[Ag(dppe)(CN\text{-}t\text{-}Bu)_2]BF_4$ (**2**) and $[Cu(dppp)(CN\text{-}t\text{-}Bu)_2]BF_4$ (**3**), and 25 s for $[Ag_2(dppp)_2](BF_4)_2$. The CCD detector distance was 5 cm. The data were reduced (SAINT)[14] and corrected for absorption (SADABS).[15] The structures were solved by direct methods and refined by full-matrix least squares on F (SHELXTL).[15,16] For $[Cu(dppe)(CN\text{-}t\text{-}Bu)_2]BF_4$ (**1**), one of the *tert*-butyl groups was disordered and the site occupancy determined using an isotropic model as 0.75 (C(34)−C(36)) and 0.25 (C(34A)−C(36A)) and fixed in subsequent refinement cycles. All non-hydrogen atoms were refined anisotropically. Hydrogen atoms were found in Fourier difference maps and refined isotropically with the exception of the hydrogen atoms in the disordered group. Hydrogen atoms of the major component were included in calculated positions and refined as a riding model C(34)−C(36). Hydrogen atoms at C(34A)−C(36A) were omitted. A rigid model does exist and means the x, y, z, and U are not refined. A riding model means the x, y, and z change as x, y, and z of the atom they are bonded to change and U is taken as 1.2−1.5 (depending on type) of U_{eq} of the atom it rides on. The hydrogen atoms of the major component were treated as a rigid model. So the hydrogen atoms at C(34)−C(36) were included in calculated positions and refined (using a rigid model), but the hydrogen atoms at C(34A)−C(36A) were omitted. For $[Ag(dppe)(CN\text{-}t\text{-}Bu)_2]BF_4$ (**2**), one of the *t*-Bu groups was disordered and the site occupancy determined using an isotropic model as 0.33 (C(8)−C(10)), 0.33 (C(8A)−C(10A), and 0.33 (C(8B)−C(10B)) and fixed in subsequent refinement cycles. All non-hydrogen atoms were refined anisotropically with the exception of the disordered *t*-Bu group. Hydrogen atoms were located in Fourier difference maps and refined isotropically with the exception of the methyl hydrogens at C(8)−C(10), C(8A)−C(10A) and C(8B)−C(10B), which were omitted. For $[Cu(dppp)(CN\text{-}t\text{-}Bu)_2]BF_4$ (**3**), the BF_4 anion and one of the *t*-Bu group was disordered and the site occupancy was determined using an isotropic model as 0.75 (F(1)−F(3)), 0.25 (F(1A)−F(3A), 0.7 (C(10)−C(12)), and 0.3 (C(10A)−C(12A)) and was fixed in the subsequent refinement cycles. All non-hydrogen atoms were refined anisotropically. Hydrogen atoms were located in Fourier difference maps and refined isotropically with the exception of the methyl hydrogens at C(6) which were included in calculated positions and refined using a riding model. Hydrogen atoms at C(10A)−C(12A) were omitted. For $[Ag_2(dppp)_2](BF_4)_2$, the BF_4 anion was disordered and the site occupancy determined using an isotropic model as 0.75 (F(2)−F(4)) and 0.25 (F(2A)−F(4A) and fixed in subsequent refinement cycles. All non-hydrogen atoms were refined anisotropically. Hydrogen atoms were located in Fourier difference maps and refined isotropically.

(14) *SAINT 6.02*; Bruker AXS, Inc.: Madison, WI, 1997−1999.
(15) Sheldrick, G. *SADABS*; Bruker AXS, Inc.: Madison, WI, 1999.
(16) Sheldrick, G. *SHELXTL 5.1*; Bruker AXS, Inc.: Madison, WI, 1997.

Chart 5

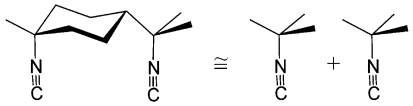

Intrinsic Viscosity. The oligomeric nature of the materials in solution was qualitatively established from the measurements of the intrinsic viscosity using the universal standard polymethyl methacrylate from Aldrich (M_n = 12 000, 15 000, 120 000, and 320 000). All measurements were repeated 5 times for greater accuracy. Although the results were checked against the known oligomer $\{[Ag(dmb)_2]BF_4\}_n$ (M_n = 4000),[4e] the results are still at the lower end of the method's accuracy. Only an approximate value of number of units can be obtained.

Computer Modeling. The calculations were performed using the commercially available PC model from Serena Software (version 7.0), which uses the MMX empirical model. No constraint on bond distances and angles was applied to ensure that deviations from normal geometry were depicted. The program sets by default a N^+ for any tetravalent nitrogen, and unrealistic intramolecular $N^+\cdots N^+$ repulsions are computed. The isocyanide group behaves as a neutral fragment. To overcome this problem, C≡N−R was replaced by the C≡C−R group. These fragments exhibit relatively the same dimension. The method was checked against X-ray data for $[M(dppe)(CN\text{-}t\text{-}Bu)_2]^+$ (M = Cu, Ag) and $[Cu(dppp)(CN\text{-}t\text{-}Bu)_2]^+$ (see text).

Results and Discussion

Model Compounds. The dppe[17] and dppp[11,18] ligands can act either as chelates or bridging species on both Cu(I) and Ag(I) ions according to the literature. Because no crystal suitable for X-ray diffraction studies has been obtained for the reported oligomers in this work and no data on complexes of the type $[M(diphos)(CNR)]^+$ are reported in the Cambridge Databank, the "chelate vs bridging" behavior has been addressed by synthesizing and characterizing the model mononuclear compounds $[M(dppe)(CN\text{-}t\text{-}Bu)_2]BF_4$ (M = Cu (**1**), Ag (**2**)) and $[Cu(dppp)(CN\text{-}t\text{-}Bu)_2]BF_4$ (**3**). This monodentate CN-*t*-Bu ligand can adequately mimic both the electronic density and steric behavior of dmb (Chart 5).The syntheses proceed from a 1:2 (M/*t*-BuNC) stoichiometric reaction between the starting materials $[M(dppe)(BF_4)]$ or $[M_2(dppp)_2](BF_4)_2$[19] and the isocyanide. These compounds crystallize easily and have been characterized by X-ray crystallography (Tables 2 and 3; Figures 1 and 2). The chelate form for these diphosphines is observed, where the 5- and 6-membered rings for the dppe and dppp species exhibit puckered and chair structures, respectively. The *t*-BuNC

(17) (a) Albano, V. C.; Bellon, P. L.; Ciani, G. *J. Chem. Soc., Dalton Trans.* **1972**, 1938. (b) Chi-Chang, L.; Yong-Shou, L.; Li, L. *Jiegou Huaxue* **1993**, *12*, 286 (also Cambridge Structural Database). (c) Saravanabharathi, D.; Monika; Venugopalan, P.; Samuelson, A. G. *Polyhedron* **2002**, *21*, 2433. (d) Semmelmann, M., Ph.D. Dissertation, Universität Karlsruhe, 1997; p 35.
(18) (a) Affandi, D.; Berners-Price, S. J.; Effendy, Harvey, P. J.; Healy, P. C.; Ruch, B. E.; White, A. H. *J. Chem. Soc., Dalton Trans.* **1997**, 1411. (b) Tiekink, E. R. T. *Acta Crystallogr.* **1990**, *46c*, 1933. (c) Brandys, M.-C.; Puddephatt, R. J. *Chem. Commun.* **2001**, 1508. (d) Xie, W.-G.; Wang, R.-W.; Xiong, Y.-F.; Yang, R.-N.; Wang, D.-M.; Jin, D.-M.; Chen, L.-R.; Luo, B.-S. *Jiegou Huaxue* **1997**, *16*, 293. See also the Cambridge Databank. (e) Ferrer, M.; Rossel, O.; Seco, M.; Soler, M.; Font-Bardia, M.; Solans, X.; de Montauzon, D. *J. Organomet. Chem.* **2000**, *598*, 215.

Table 2. Crystallographic Data for **1**−**3**

	[Cu(dppe)(CN-*t*-Bu)$_2$](BF$_4$) (**1**)	[Cu(dppp)(CN-*t*-Bu)$_2$](BF$_4$) (**3**)	[Ag(dppe)(CN-*t*-Bu)$_2$](BF$_4$) (**2**)
formula	$C_{36}H_{42}BCuF_4N_2P_2$	$C_{37}H_{44}BCuF_4N_2P_2$	$C_{36}H_{42}AgBF_4N_2P_2$
fw	715.01	729.03	759.34
cryst size	0.28 × 0.45 × 0.50	0.25 × 0.30 × 0.40	0.40 × 0.45 × 0.45
lattice	monoclinic	monoclinic	monoclinic
space group	$P2_1/n$	$P2_1/c$	$P2_1/n$
a, Å	14.0252(15)	15.5433(9)	14.1130(8)
b, Å	10.2034(11)	11.2094(6)	10.2075(6)
c, Å	25.515(2)	21.4362(12)	25.8175(16)
α, deg	90	90	90
β, deg	103.765(2)	92.483(1)	103.381(1)
γ, deg	90	90	90
V, Å^3	3546.4(6)	3731.3(4)	3618.3(4)
Z	4	4	4
ρ(calcd), g cm^{-3}	1.339	1.298	1.394
F(000)	1488	1520	1560
μ(Mo Kα), mm^{-1}	0.755	0.719	0.693
temp, K	198(1)	173(1)	173(1)
R1[a]	0.0289	0.0327	0.0292
wR2[b]	0.0785	0.0976	0.0828
no. of observns ($I > 2.00\sigma(I)$)	6101	8479	8217
no. of variables	577	642	556

[a] $R1 = \sum||F_o| - |F_c||/\sum|F_o|$. [b] $wR2 = (\sum[w(F_o^2 - F_c^2)^2]/\sum[F_o^4])^{1/2}$. Weight for **1** = $1/[\sigma^2(F_o^2) + (0.0463P)^2 + (1.7267P)]$, weight for **2** = $1/[\sigma^2(F_o^2) + (0.0498P)^2 + (1.9892P)]$, and weight for **3** = $1/[\sigma^2(F_o^2) + (0.0569P)^2 + (0.6494P)]$, where $P = (\max(F_o^2, 0) + 2F_c^2)/3$.

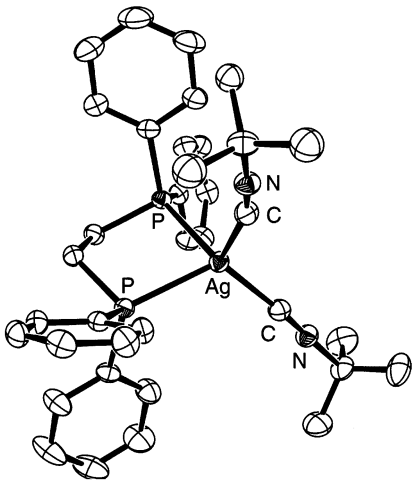

Figure 1. Molecular structure for [Ag(dppe)(CN-*t*-Bu)$_2$]BF$_4$ (**2**). The ellipsoids are shown at 30% probability. The H atoms and BF$_4^-$ ion are not shown for clarity. The compound is isostructural to [Cu(dppe)(CN-*t*-Bu)$_2$]BF$_4$ (**1**) (see Supporting Information).

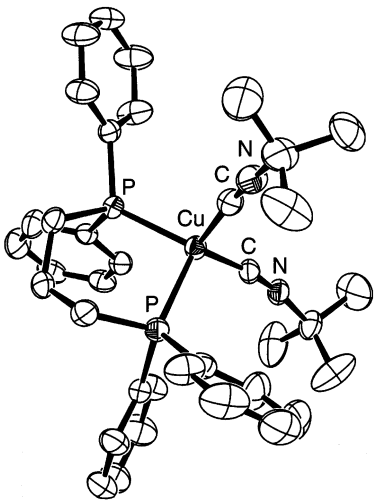

Figure 2. Molecular structure for [Cu(dppp)(CN-*t*-Bu)$_2$]BF$_4$ (**3**). The ellipsoids are shown at 30% probability. The H atoms and the BF$_4^-$ ion are not shown for clarity.

ligands coordinate the two remaining tetrahedral positions of the M atoms, and the M−P, M−C, and C≡N distances are normal (Table 3). Some deviations from linearity of the MCN angles, which are on average 173 and 169° for M = Cu and Ag in the [M(dppe)(CN-*t*-Bu)$_2$]BF$_4$ complexes, respectively, and 172° for [Cu(dppp)(CN-*t*-Bu)$_2$]BF$_4$, are observed. The PMP and CMC angles are smaller and greater, respectively, than the ideal tetrahedral angle, due to the smaller bite angle of the chelating diphos ligand.

The model compounds [Pd$_2$(diphos)$_2$(CN-*t*-Bu)$_2$](ClO$_4$)$_2$ (diphos = dppe (**4**), dppp (**5**)) were prepared in one step from the starting Pd$_2$(CN-*t*-Bu)$_4$Cl$_2$ complex (Scheme 1).

Other related d^9−d^9 Pd$_2$ dimers have been reported in the literature including the M$_2$(diphos)$_2$(CNR)$_2^{2+}$ complexes and the Pd$_2$(dppp)$_2^{2+}$ species, where M = Pd or Pt and R = Me, 2,4,6-Me$_3$C$_6$H$_2$, and 2,6-Me$_2$C$_6$H$_3$.[20] Their structures consist of an unsupported Pd−Pd bond with two square planar Pd fragments forming angles of 84−88°.[20] The two diphosphine ligands are chelating each of the Pd atoms via one of the equatorial and the axial positions. The remaining equatorial coordination sites are occupied by the isocyanide ligands.

No crystal suitable for X-ray analysis was obtained for the dimers in this work. The ^{31}P NMR spectra exhibit 2 resonances associated with P atoms coordinated at the axial and equatorial positions. The ^2J(P, P) values are very small,

(19) The dication is isostructural to Au$_2$(dppp)$_2^{2+}$: Brandys, M.-C.; Puddephatt, R. J. *Chem. Commun.* **2001**, 1280. Moreover, a distinctive difference is noticed in Ag−P distances (2.3797(4) and 2.3890(4) Å) between the unsaturated Ag$_2$(dppp)$_2^{2+}$ cation (shorter than 0.1 Å) and the saturated Ag(dppe)(CN-*t*-Bu)$_2^+$ species. An electronic effect is likely to be at the origin for this difference. In addition, the PAgP angle (159°) strongly deviates from linearity, witnessing the important Ag$^+$···F−BF$_3^-$ interactions.

(20) (a) Tanase, T.; Kawahara, Ukaji, H.; Kobayashi, K.; Yamazaki, H.; Yamamoto, Y. *Inorg. Chem.* **1993**, *32*, 3682. (b) Tanase, T.; Ukaji, H.; Kudo, Y.; Ohno, M.; Kobayashi, K.; Yamamoto, Y. *Organometallics* **1994**, *13*, 1374. (c) Lindsay, C. H.; Benner, L. S.; Balch, A. L. *Inorg. Chem.* **1980**, *19*, 3503. (d) Budzelaar, P. H. M.; van Leeuwen, P. W. N. M.; Roobeek, C. F. *Organometallics* **1992**, *11*, 23.

Table 3. Selected Bond Distances (Å) and Angles (deg) for **1**−**3**

	[Cu(dppe)(CN-*t*-Bu)$_2$]BF$_4$ (**1**)	[Ag(dppe)(CN-*t*-Bu)$_2$]BF$_4$ (**2**)	[Cu(dppp)(CN-*t*-Bu)$_2$]BF$_4$ (**3**)
d(MP)	2.2979(5)	2.4939(5)	2.2636(4)
	2.3038(5)	2.4982(5)	2.2898(5)
d(MC)	1.9245(18)	2.145(2)	1.9176(18)
	1.9306(18)	2.1719(19)	1.935(2)
d(CtN)	1.144(2)	1.141(3)	1.142(2)
	1.145(2)	1.139(3)	1.132(3)
∠PMP	89.088(17)	84.504(16)	98.737(17)
∠CMC	120.19(1)	119.67(8)	113.54(8)
∠CMP	112.39(5)	114.21(6)	118.98(5)
	108.35(5)	108.57(6)	110.63(6)
	116.61(5)	118.28(5)	108.61(5)
	105.69(5)	106.01(6)	104.22(6)
∠MCN	175.55(16)	174.96(18)	170.86(15)
	170.33(16)	163.54(18)	172.85(18)

Scheme 1

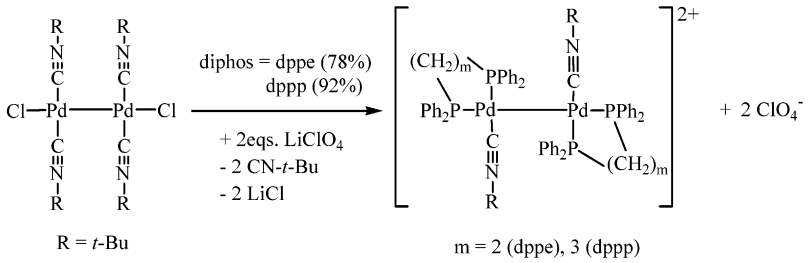

which are consistent with two interacting ^{31}P nuclei forming a PPdP angle of ∼90°. The UV−visible spectra also exhibit a strong absorption at ∼414 nm, characteristic of the presence of a Pd−Pd bond (discussed below).

dmb Oligomers. The colorless Cu and Ag materials are obtained by reacting the corresponding starting [M(dppe)(BF$_4$)] or [M$_2$(dppp)$_2$](BF$_4$)$_2$ materials with dmb in excess. The yellow Pd$_2$ polymers are obtained differently by reacting the d^9−d^9 dimer Pd$_2$(dmb)$_2$Cl$_2$ with 2 equiv of dppe or dppp according to

$$Pd_2(dmb)_2Cl_2 + 2diphos \rightarrow (1/n)Pd_2(diphos)_2(dmb)^{2+}{}_n + dmb + 2Cl^- \quad (1)$$

where diphos is dppe (**10**; 79% yield) or dppp (**11**; 86% yield). The close similarity in the ^{31}P NMR, IR, and UV−vis spectra between the model compounds and the oligomers suggests that the "Pd$_2$(diphos)$_2$(CNR)$_2^{2+}$" unit is present in the materials, including the chelate structure of the "Pd(diphos)" fragment.

All investigated dmb-containing materials are amorphous according to the XRD patterns (see examples in the Supporting Information), and no crystal suitable for single-crystal X-ray studies was obtained despite numerous attempts.

The TGA traces for both the *t*-BuNC model compounds and dmb-containing materials indicate two thermal events. The low-temperature event corresponds to the loss of the isocyanides, and the higher temperature event, to the loss of the diphosphines and counteranion (see Supporting Information for details). The weight losses are consistent with the isocyanide/diphosphine/counterion ratio, taking into account the uncertainties. The comparison between the *t*-BuNC model compounds and dmb-containing materials indicates that the *t*-BuNC ligand is generally lost at a lower temperature with respect to the dmb analogues (see Figure 3 as an example, Supporting Information). For instance, the first weight loss for [Cu(dppe)(CN-*t*-Bu)$_2$]BF$_4$ (**3**) occurs in the 160−224 °C window, while it occurs at 178−334 °C for {[Cu(dppe)(dmb)]BF$_4$}$_n$ (**6**). The first derivative traces exhibit inflection points at 201.4 and 211.6 °C for [Cu(dppe)(CN-*t*-Bu)$_2$]BF$_4$ (**3**) and {[Cu(dppe)(dmb)]BF$_4$}$_n$ (**6**), respectively.

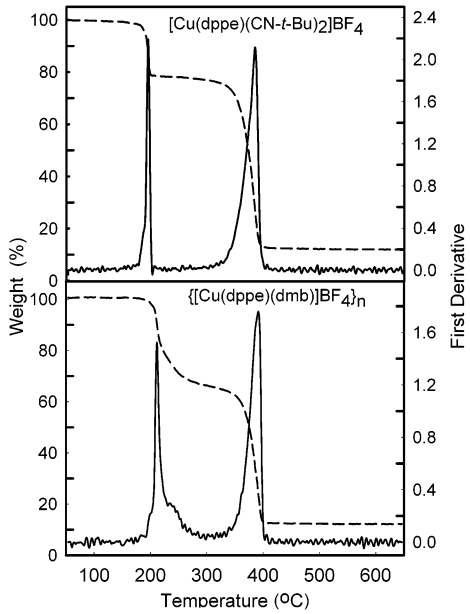

Figure 3. TGA traces for [Cu(dppe)(CN-*t*-Bu)$_2$]BF$_4$ (**1**, up) and {[Cu(dppe)(dmb)]BF$_4$}$_n$ (**6**, down). The broken line is the first derivative of the TGA traces.

The intrinsic viscosity measurements indicate that the M_n values for {[Pd$_2$(dppe)$_2$(dmb)](ClO$_4$)$_2$}$_n$ and {[Pd$_2$(dppp)$_2$(dmb)](ClO$_4$)$_2$}$_n$ are 11 800 and 12 200 (±200), respectively. The average number of Pd$_2$ units is ∼8−9. Similarly, the {[Cu(diphos)(dmb)]BF$_4$}$_n$ materials exhibit M_n of (dppe, **6**;

Chart 6

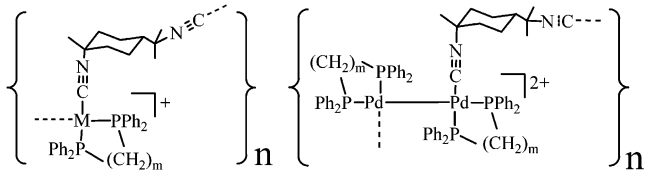

M = Cu, Ag; m = 2, 3 m = 2, 3

6570) and (dppp, **8**; 6870), which also indicate the presence of oligomers. Conversely, the Ag materials dissolve far more rapidly than those of Cu and Pd_2 species, and their corresponding acetonitrile solutions exhibit no time difference with the pure solvent. This result indicates the presence of extensively dissociated materials in solution. All in all, the data are consistent with the formulation shown in Chart 6 for these new materials.

The chemical analysis and the integration of the ^{1}H NMR signals are consistent with the 1:1.*x* diphos/dmb stoichiometries for the $\{M(diphos)(dmb)^+\}_n$ (M = Cu, Ag) oligomers, where *x* is a small number (~1−2) and is due to the presence of dmb acting as end-of-chain units. The presence of weak IR peaks associated with uncoordinated C≡NR groups (~2130 cm^{-1}) is noted for the Ag-containing oligomers in the solid state, which is consistent with end-of-chain dmb units. For the $\{Cu(diphos)(dmb)^+\}_n$ (**6** and **8**) and $\{Pd_2(diphos)_2(dmb)^{2+}\}_n$ materials (**10** and **11**), there is no evidence for such an IR peak in the solid state, suggesting that the signal may be weak or the oligomers may be cyclic.

Using the spin-coating technique, or by simply evaporating an acetonitrile solution, these 6 materials form clear films with no sign of a heterogeneous area under the microscope. While the films formed by the Ag oligomers are found to be brittle, stand-alone films are obtained for the Cu and Pd_2 materials. In one case, $\{[Cu(dppe)(dmb)]BF_4\}_n$ (**6**), a glass transition at T_g = 81.5 °C (ΔC_p = 0.43 J/(g deg)) is reproducibly observed in the DSC traces.

The Pd_2 materials belong to a broader family of organometallic oligomers, which contains unsupported M_2 bonds in the backbone. The number of examples is still somewhat limited,[21] but the incorporation of a Pd_2 bond is, to our knowledge, unprecedented.

Computer Modeling. Modeling is used to qualitatively address two issues. The first one concerns why oligomer structures are favored in this work, while, in other related complexes, dimer species are observed. The second one concerns what we can extract from the computed structures in terms of predicted properties. The first series of computations deals with the comparison between computed and X-ray structures of related Cu, Ag, and Pd_2 complexes, providing a degree of reliability of the method employed. These complexes are the three model Cu and Ag complexes described above and the X-raycharacterized $Pd_2(dmb)_2Cl_4$[9c] and $[Pd(dppe)(dmb)]_2^{4+}$ (Chart 7).[22]

Chart 7

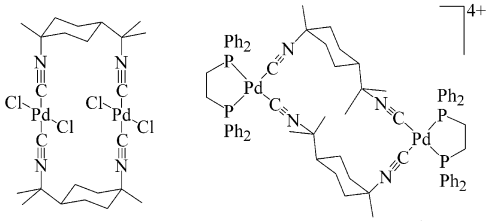

$Pd_2(dmb)_2Cl_4$ $[Pd(dppe)(dmb)]_2^{4+}$

The comparison between MMX and X-ray data for the $M(diphos)(CN\text{-}t\text{-}Bu)_2^+$ complexes is presented in Table 4. The computations give satisfactory results in M−P distances (the largest difference is 0.07 Å, 2.8%) and skeleton angles (the largest difference is ~5°, but usually it is ~1°) for the Cu complexes, but worse comparisons are noticed for the Ag species. The M−C and C≡N distances are respectively under- and overestimated. Their sums, however, provide a better comparison. Similar observations are made for the $Pd_2(dmb)_2Cl_4$ and $[Pd_2(dppe)(dmb)]_2^{4+}$ complexes,[22] where bond lengths and angles are well reproduced in the calculations, except that the Pd−P distance is somewhat off. The distance is longer by about 0.1 Å.

The structures for the chiral $Pd_2(diphos)_2(CN\text{-}t\text{-}Bu)_2^{2+}$ complexes (diphos = dppe (**4**), dppp (**5**)) have been modeled as well (see Figure 4 for example). The computed Pd−Pd (2.66), Pd−P_{ax} (2.36), Pd−P_{eq} (2.36), and Pd−C (1.89 Å) distances compare reasonably well with those found experimentally for the corresponding aryl species (2.60−2.62, 2.32−2.36, 2.30−2.33, 1.96−1.97 Å, respectively).[20] The computed structures exhibit a twisted geometry where the dihedral angle (CPdPdC) is about 77−78°, an angle that is smaller than those seen for the above compounds (86°).[20] This difference reflects the presence of greater steric hindrance for the *tert*-butyl groups in comparison with the diphos-phenyl fragments. Full rotation about the Pd−Pd bond is severely hindered, so inversion of configuration is impossible.

The replacement of the two *t*-BuNC groups in these computed models by one dmb bridging ligand generates the dinuclear "$Pd_2(diphos)_2(dmb)^{2+}$" complex, where the Pd−Pd bond is now supported by a dmb ligand (Figure 5). While most distances remained unchanged, significant changes are noted in PdCN (158−169°), and dihedral angles (~73°), witnessing significant ring stress. In addition, the PPdPdP axis now exhibits a pronounced arch where the PPdPd angles are in the range of 160°. This structure is not favored.

Similarly, the tetranuclear structure for "$[Pd_2(diphos)_2(dmb)]_2^{4+}$" exhibits a macrocycle composed of two Pd−Pd−(*Z*-dmb) units where the two Pd−Pd axes are placed parallel to each other (Figure 6). Although no major distortions are noted in the structure, the dmb ligand is found quasi-

(21) (a) Tenhaeff, S. C.; Tyler, D. R. *Organometallics* **1991**, *10*, 473. (b) Tenhaeff, S. C.; Tyler, D. R. *J. Chem. Soc., Chem. Commun.* **1989**, 1459. (c) Tenhaeff, S. C.; Tyler, D. R. *Organometallics* **1992**, *11*, 1466. (d) Tenhaeff, S. C.; Tyler, D. R. *Organometallics* **1991**, *10*, 1116. (e) Male, J. L.; Lindsfors, B. E.; Covert, J.; Tyler, D. R. *Macromolecules* **1997**, *30*, 6404. (f) Nieckarz, G. F.; Tyler, D. R. *Inorg. Chim. Acta* **1996**, *242*, 303. (g) Male, J. L.; Yoon, M.; Glenn, A, G.; Weakly, T. J. R.; Tyler, D. R. *Macromolecules* **1999**, *32*, 3898. (h) Nieckarz, G. F.; Litty, J. J.; Tyler, D. R. *J. Organomet. Chem.* **1998**, *554*, 19.

(22) The X-ray structure for $[Pd(dppe)(dmb)]_2(PF_6)_4$ will be reported elsewhere: Fortin, J.-F.; Harvey, P. D. To be published.

Table 4. Comparison of MMX and X-ray Data for **1**−**3**, $Pd_2(dmb)_2Cl_4$, and $[Pd(diphos)(dmb)]_2^{4+}$ Complexes[a]

	Cu(dppe)(CN-*t*-Bu)$_2^+$ (**1**)	Cu(dppp)(CN-*t*-Bu)$_2^+$ (**3**)	Ag(dppe)(CN-*t*-Bu)$_2^+$ (**2**)
d(M-P), Å	2.27 (2.30)	2.27 (2.28)	2.43 (2.50)
d(M-C), Å	1.82 (1.93)	1.82 (1.92)	1.99 (2.16)
d(CtN), Å	1.19 (1.15)	1.19 (1.14)	1.18 (1.14)
∠(PMP), deg	85.2 (89.1)	93.7 (98.7)	79.4 (84.5)
∠(CMC), deg	121.4 (120.2)	118.6 (119.7)	122.0 (119.7)
∠(MCN), deg	171.6 (172.8)	172.5 (171.9)	171.7 (169.3)
∠(PMC), deg	110.7 (110.8)	110.9 (110.9)	108.0 (118.8)
	$Pd_2(dmb)_2Cl_4$[b]	$[Pd(dppe)(dmb)]_2^{4+}$[c]	$[Pd(dppp)(dmb)]_2^{4+}$
d(Pd−P), Å		2.38 (2.27)	2.38
d(Pd−C), Å	1.93 (1.97)	1.93 (2.02)	1.93
d(CtN), Å	1.14 (1.13)	1.20 (1.13)	1.20
∠(PPdP), deg		78.9 (82.7)	82.7
∠(CPdC), deg	178.0 (178.6)	92.5 (90.6)	94.2
∠(PdCN), deg	177.5 (178.6)	174.3 (176.0)	174.0
∠(PPdC), deg[d]		94.3 (93.4)	91.6

[a] The X-ray data are placed in parentheses and are from this work unless stated otherwise. [b] From ref a. [c] From ref b. [d] Only the angles approaching 90° of the square planar geometry are provided.

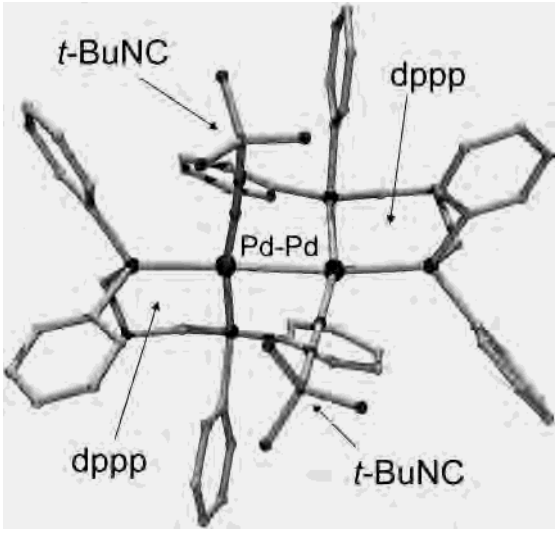

Figure 4. Computer model for $Pd_2(dppp)_2(CN\text{-}t\text{-}Bu)_2^{2+}$ (**5**). The ClO_4^- ion is not shown.

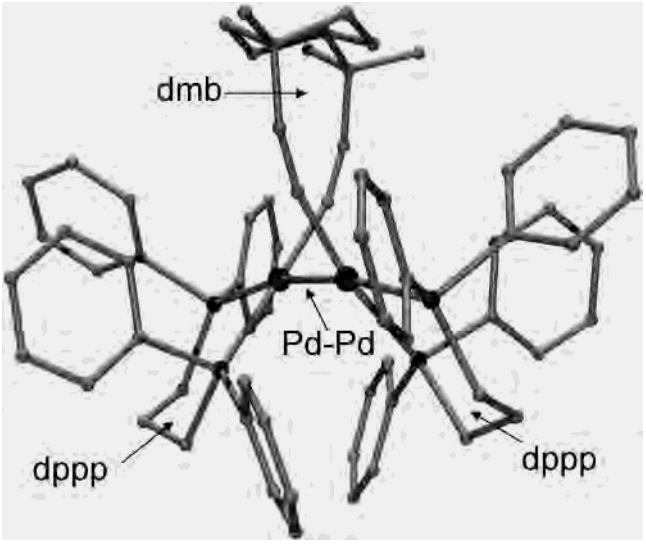

Figure 5. Computer modeling of a fictitious dimer $Pd_2(dppp)_2(dmb)^{2+}$. The stress in the "$Pd_2(dmb)$" ring makes this structure improbable.

encapsulated between the four diphos chelates pressed between the phenyl groups. Numerous C−H···H−C contacts (2.257, 2.268 and 2.408 Å, for the structure shown in Figure 6) are noted indicating the presence of some steric interactions. These interactions are also felt by a small increase in calculated $Pd-P_{ax}$ distances (from 2.38 to 2.39−2.40 Å) and a small deviation of the $PdPdP_{ax}$ angles (∼169° in comparison with ∼174° calculated for the model compounds $Pd_2(diphos)_2(CN\text{-}t\text{-}Bu)_2^{2+}$; Figure 4).

On the other hand, the computed models for the $\{Pd_2(diphos)_2(dmb)^{2+}\}_n$ oligomers (see Figure 7 as an example) exhibit dmb ligands in their gauche conformation that are significantly less encapsulated than the above dimer and phenyl groups with no or a few close C−H···H−C contacts. For instance, the shortest C−H···H−C distance is 2.487 Å in this case. The average computed PdCN angles are ∼176.5°. In addition, multiple conformations (relative orientation of Pd_2 units with respect to each other) are possible, where the Pd−Pd bonds are never found parallel to each other. Computations performed on 3 identical (same stereoisomer) or different units (both enantiomers) show that stereoregularity seems impossible at least for short fragments. This result may explain the amorphous morphology observed (XRD) for the solid material.

The structure of a cyclic "$Cu_2(diphos)_2(dmb)_2^{2+}$" dimer has also been examined and consists of a similar geometry to the $[Pd(dppe)(dmb)]_2^{4+}$ discussed above. The difference is that the CMC angle is tetrahedral instead of 90°. This macrocycle exhibits some ring stress (see Supporting Information). For instance, the computed PdCN angles range from 165 to 171° in comparison with computed angles of 172.5° for the mononuclear Cu(dppp)(CN-*t*-Bu)$_2^+$ (**3**) (Table 4). This result contrasts greatly with the d^8-d^8 compound $[Pd(dppe)(dmb)]_2^{4+}$ and suggests that a simple increase in CMC angle from 90 to 109.5° is enough to create a ring stress and to drive the oligomer formation.[23]

Electronic Spectra. The $\{[M(diphos)(dmb)]BF_4\}_n$ and $[M(diphos)(CN\text{-}t\text{-}Bu)_2]BF_4$ species (M = Cu, Ag; diphos =

(23) The computed segments for $\{Cu(dppp)(dmb)^+\}_n$ exhibit an average PdCN angle of 175° indicating the absence of stress in the chain.

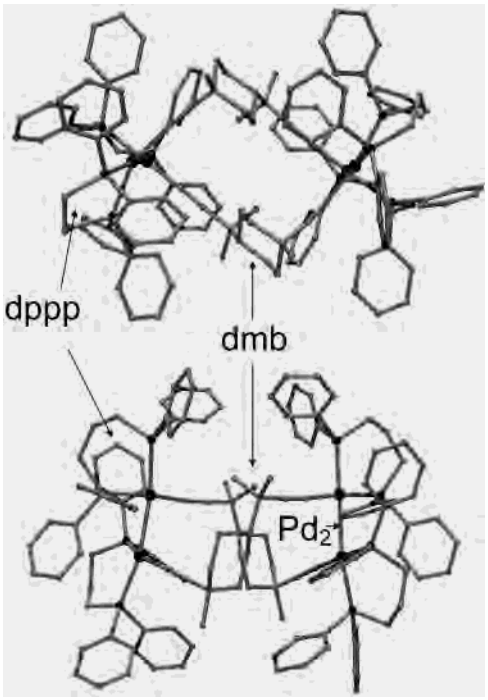

Figure 6. Top and side view of a computer model for the fictitious $[Pd_2(diphos)_2(dmb)]_2^{4+}$ complex. This structure exhibits close C−H···H−C contacts.

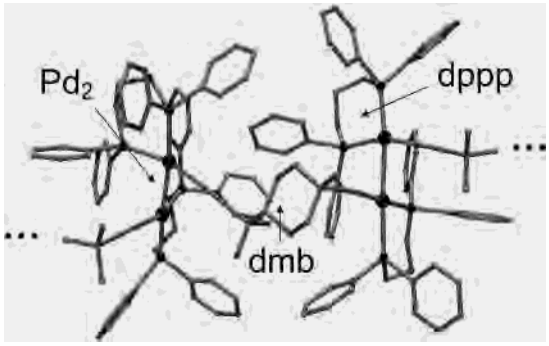

Figure 7. Computer model for a fragment of the $\{Pd_2(dppp)_2(dmb)^{2+}\}_n$ oligomer (**10**). This is one possible conformation and one pair of the same enantiomer. Other combinations exist. The ClO_4^- ion is not shown.

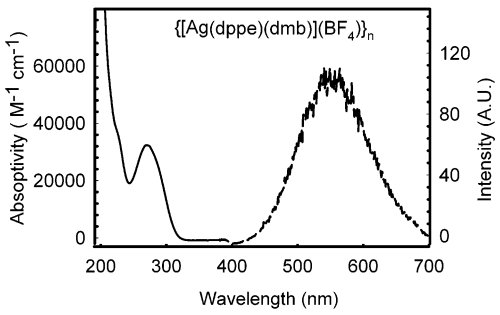

Figure 8. UV−vis spectra (left-hand side) for $\{[Ag(dppe)(dmb)]BF_4\}_n$ (**7**) in acetonitrile at 298 K and solid-state emission spectra (right-hand side) for the same material at 298 K.

dppe, dppp; **1**−**3**, **6**−**9**) exhibit a structureless low-energy absorption at 272 ± 2 nm, with absorptivities ranging from 23 000 to 34 000 M^{-1} cm^{-1}(see Experimental Section for data and Figure 8 as an example). This electronic band is assigned to a metal-to-ligand charge transfer (MLCT), where the ligand manifold comprises both the π-systems of the C≡N and PPh_2 groups. This assignment is based on the recent theoretical findings (EHMO and DFT) and spectroscopic experimental data for the mixed-ligand related dimer complex $[Cu_2(dppm)_2(O_2CMe)]^+$ [24] and the monomer $[M(CN\text{-}t\text{-}Bu)_4]^+$.[4b]

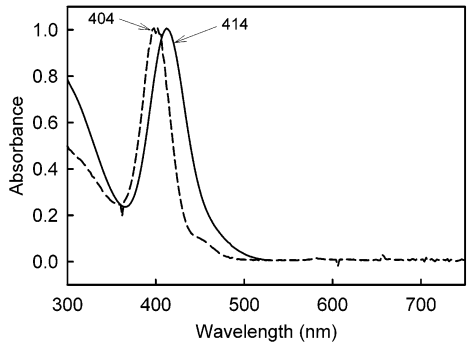

Figure 9. Comparison of the UV−vis spectra of $\{[Pd_2(dppe)_2(dmb)](ClO_4)_2\}_n$ (**10**) in PrCN at 298 (—) and 77 K (---).

The electronic absorption spectra for the $Pd_2(diphos)_2(CN\text{-}t\text{-}Bu)_2^{2+}$ model compounds and the $\{Pd_2(diphos)_2(dmb)^{2+}\}_n$ polymers in PrCN exhibit narrow featureless absorptions at 293 K at 420 (**4**) and 414 nm (**5**) for the dimers and at 428 (**10**) and 416 nm (**11**) for the polymers with diphos = dppe and dppp, respectively (see Figure 9 as an example). These values are slightly blue-shifted with respect to the starting material $Pd_2(dmb)_2Cl_2$ (444 nm) but compare favorably with that of the related d^9-d^9 dimer $Pd_2(dppm)_2Cl_2$ (418 nm).[26] This absorption is easily assigned to $d\sigma \rightarrow d\sigma^*$ as previously demonstrated by Sourisseau and co-workers for $Pd_2(dppm)_2Cl_2$ (by resonance Raman spectroscopy),[25] and by this group for $Pd_2(dmb)_2Cl_2$ (EHMO,[26] DFT,[27] and FT-Raman spectroscopy second moment band analysis[26]). The electronic bands associated with $d\sigma \rightarrow d\sigma^*$ electronic transitions for M_2-bonded species generally exhibit low energy, high intensity (ϵ > 25 000 M^{-1} cm^{-1}; Table 5), and small fwhm (full width at half-maximum; 2200 < fwhm < 2700 cm^{-1} at 293 K), as seen for these two materials (2540 and 2670 cm^{-1} for the dppe and dppp species, respectively). Upon cooling of the $\{Pd_2(diphos)_2(dmb)^{2+}\}_n$-containing solution from 293 to 77 K, the λ_{max} and fwhm of the $d\sigma \rightarrow d\sigma^*$ bands decrease slightly down to 424 and 406 nm and 2500 and 2300 cm^{-1} for dppe (**10**) and dppp (**11**), respectively.

Solid-State Luminescence. The $M(diphos)(CN\text{-}t\text{-}Bu)_2^+$ model compounds (**1**−**3**) and $\{M(diphos)(dmb)^+\}_n$ polymers (M = Cu, Ag; diphos = dppe, dppp; **6**−**9**) exhibit broad luminescence found between ~480 and 550 nm in the solid state (Figure 8). The Stokes shift is very large (>17 000 cm^{-1}), and the emission lifetimes range in the microsecond time scale (18 < τ_e < 48 μs; see detail in Table 6). This experimental evidence indicates that the emission is phosphorescence. These emission maxima and lifetimes compare

(24) Harvey, P. D.; Drouin, M.; Zhang, T. *Inorg. Chem.* **1997**, *36*, 4998.
(25) Alves, O. L.; Virtoge, M.-C.; Sourisseau, C. *Nouv. J. Chim.* **1983**, *7*, 231.
(26) Harvey, P. D.; Murtaza, Z. *Inorg. Chem.* **1993**, *32*, 4721.
(27) Provencher, R.; Harvey, P. D. *Inorg. Chem.* **1996**, *35*, 2113.

Table 5. UV−Vis Data for **4**, **5**, **10**, and **11**

compds	ACN/293 K		PrCN/293 K		PrCN/77 K	
	λ_{max} (nm)	ϵ (M^{-1} cm^{-1})	λ_{max} (nm)	fwhm (cm^{-1})	λ_{max} (nm)	fwhm (cm^{-1})
$[Pd_2(dppe)_2(CN\text{-}t\text{-}Bu)_2](ClO_4)_2$ (**4**)	420	28 600	422	2200	416	1800
$[Pd_2(dppp)_2(CN\text{-}t\text{-}Bu)_2](ClO_4)_2$ (**5**)	416	26 000	418	2100	410	1900
$\{[Pd_2(dppe)_2(dmb)](ClO_4)_2\}_n$ (**10**)	418	28 000	420	2700	424	2500
$\{[Pd_2(dppp)_2(dmb)](ClO_4)_2\}_n$ (**11**)	414	26 100	416	2500	406	2300

Table 6. Solid-State Emission Data for the $M(diphos)(CN\text{-}t\text{-}Bu)_2^+$ Model Compounds and $\{M(diphos)(dmb)^+\}_n$ Oligomers

compds	λ_{max} emission (nm)	τ_e (μs)
$[Cu(dppe)(CN\text{-}t\text{-}Bu)_2](BF_4)$ (**1**)	540	42 ± 4
$[Ag(dppe)(CN\text{-}t\text{-}Bu)_2](BF_4)$ (**2**)	515	21 ± 4
$[Cu(dppp)(CN\text{-}t\text{-}Bu)_2](BF_4)$ (**3**)	478	18 ± 3
$\{[Cu(dppe)(dmb)](BF_4)\}_n$ (**6**)	480	38 ± 5
$\{[Ag(dppe)(dmb)](BF_4)\}_n$ (**7**)	548	27 ± 2
$\{[Cu(dppp)(dmb)](BF_4)\}_n$ (**8**)	500	22 ± 4
$\{[Ag(dppp)(dmb)](BF_4)\}_n$ (**9**)	480	48 ± 4

favorably to those of other tetravalent mononuclear,[4b,28] dinuclear,[29,30] trinuclear,[29,31] and polynuclear species.[29,32] The emissive excited state responsible for the emission in these cases is assigned to a ^{3}MLCT as described above.

Conversely, the $Pd_2(diphos)_2(CN\text{-}t\text{-}Bu)_2^{2+}$ (**4** and **5**) and $\{Pd_2(diphos)_2(dmb)^{2+}\}_n$ (**10** and **11**) species are found to be nonluminescent at 293 K in the solid state. This lack of luminescence has also been observed for other d^9-d^9 dimers such as $Pd_2(dppm)_2Cl_2$ and $Pd_2(dmb)_2Cl_2$, for example.[33] This behavior has been discussed previously in terms of an efficient photoinduced homolytic Pd−Pd bond cleavage, followed by a diradical recombination.[26]

Concluding Remarks. The bridging ligand dmb exhibits a very strong tendency to assemble metallic fragments to provide organometallic oligomeric materials. This observation greatly conflicts with most works reported on this ligand in the literature, where dimeric species are frequently observed.[1] The fact that many of these materials are amorphous renders their reliable characterization very difficult and contributes to the lower number of literature reports on dmb-containing materials with respect to the dimer counterparts. This paper reports another strategy for the synthesis of dmb-based organometallic polymers, which consists of using bulky metallic fragments such as the $Pd_2(diphos)_2$ units. Steric hindrance prevents dmb from bridging the Pd_2 bond (presumably due to a large unfavorable twist CPdPdC angle) and also from making the unobserved dimer $[Pd_2(diphos)_2(dmb)^{+2}]_2$.

Acknowledgment. This research was supported by the Natural Sciences and Engineering Research Council of Canada (NSERC).

Supporting Information Available: Pictures showing the computed structures for the fictitious $[Pd_2(diphos)_2(dmb)]_2^{4+}$ and $[Pd_2(diphos)_2(dmb)]_2^{4+}$ complexes, XRD patterns for the $\{[Ag(diphos)(dmb)]BF_4\}_n$ polymers (diphos = dppe, dppp), a table gathering the TGA data, and X-ray crystallographic files for $[M(dppe)(CN\text{-}t\text{-}Bu)_2]BF_4$ (M = Cu (**1**), Ag (**2**)) and $[Cu(dppp)(CN\text{-}t\text{-}Bu)_2]BF_4$ (**3**) in CIF format. This material is available free of charge via the Internet at http://pubs.acs.org.

IC034780Z

(28) (a) Simon, J. A.; Palke, W. E.; Ford, P. C. *Inorg. Chem.* **1996**, *35*, 6413. (b) Crane, D. R.; DiBenedetto, J.; Palmer, C. E. A.; McMillin, D. R.; Ford, P. C. *Inorg. Chem.* **1988**, *27*, 3698.

(29) Ford, P. C.; Cariati, E.; Bourassa, *J. Chem. Rev.* **1999**, *99*, 3625 and the references therein.

(30) Piché, D.; Harvey, P. D. *Can J. Chem.* **1994**, *72*, 705.

(31) Wang, C.-F.; Peng, S.-M.; Chan, C.-K.; Che, C.-M. *Polyhedron* **1996**, *15*, 1853.

(32) (a) Cariati, E.; Roberto, D.; Ugo, R.; Ford, P. C.; Galli, S.; Sironi, A. *Chem. Mater.* **2002**, *14*, 5116. (b) Herary, M.; Wootton, J. L.; Khan, S. I.; Zink, J. I. *Inorg. Chem.* **1997**, *36*, 796. (c) Lai, D. C.; Zink, J. I. *Inorg. Chem.* **1993**, *32*, 2594. (d) Henary, M.; Zink, J. I. *Inorg. Chem.* **1991**, *30*, 3111.

(33) The $Pd_2(dmb)_2Cl_2$ complex weakly lumineses in solution at 77 K (λ_{max} = 625 nm; $\tau_e = 71 \pm 6$ ns).[23] The $Pd_2(diphos)_2(CN\text{-}t\text{-}Bu)^{2+}$ and $\{Pd_2(diphos)_2(dmb)^{2+}\}_n$ species also show some luminescence in solution at 77 K between 510 and 560 nm with τ_e in the nanosecond time scale as well.